Proteomics-based analysis of invasion-related proteins in malignant gliomas

Running title: Proteomics-based analysis of glioma invasion

Tomoko Maruo,[1] Tomotsugu Ichikawa,[1] Hirotaka Kanzaki,[2] Satoshi Inoue,[1] Kazuhiko Kurozumi,[1] Manabu Onishi,[1] Koichi Yoshida,[1] Hirokazu Kambara,[1] Mamoru Ouchida,[2] Kenji Shimizu,[2] Seiji Tamaru,[3] E. Antonio Chiocca[4] and Isao Date[1]

[1] Department of Neurological Surgery and [2] Department of Molecular Genetics, Okayama University Graduate School of Medicine, Dentistry, and Pharmaceutical Sciences, 2-5-1, Shikata-cho, Kita-ku, Okayama, 700-8558, Japan

[3] Central Research Laboratory, Okayama University Medical School, 2-5-1, Shikata-cho, Kita-ku, Okayama, 700-8558, Japan

[4] Department of Neurosurgery, Brigham and Women's/ Faulkner Hospital, 75 Francis Street, Boston, MA, 02116, USA

Corresponding author contact information:

Tomotsugu Ichikawa, MD, PhD

Department of Neurological Surgery, Okayama University Graduate School of Medicine, Dentistry and Pharmaceutical Sciences

Address: 2-5-1, Shikata-cho, Kita-ku, Okayama, 700-8558, Japan

Phone: 81-86-235-7336; Fax: 81-86-227-0191

E-mail: tomoichi@cc.okayama-u.ac.jp

ABSTRACT

One of the insidious biological features of gliomas is potential to invade normal brain tissue extensively, yet molecular mechanisms that dictate this locally invasive behavior remain poorly understood. To investigate the molecular basis of invasion by malignant gliomas, proteomic analysis was performed using a pair of canine glioma subclones—J3T-1 and J3T-2—that show different invasion phenotypes in rat brains but have similar genetic backgrounds. Two-dimensional protein electrophoresis of whole-cell lysates of J3T-1 (angiogenesis-dependent invasion phenotype) and J3T-2 (angiogenesis-independent invasion phenotype) was performed. Twenty-two distinct spots were recognized when significant alteration was defined as more than 1.5-fold change in spot intensity between J3T-1 and J3T-2. Four proteins that demonstrated increased expression in J3T-1, and 14 proteins that demonstrated increased expression in J3T-2 were identified using liquid chromatography-mass spectrometry analysis. One of the proteins identified was annexin A2, which was expressed at higher levels in J3T-1 than in J3T-2. The higher expression of annexin A2 in J3T-1 was corroborated by quantitative reverse transcription-PCR of the cultured cells and immunohistochemical staining of the rat brain tumors. Moreover, immunohistochemical analysis of human glioblastoma specimens showed that annexin A2 was expressed at high levels in the tumor cells that formed clusters around dilated vessels. These results reveal differences in the proteomic profiles between these two cell lines that might correlate with their different invasion profiles. Thus,

annexin A2 may be related to angiogenesis-dependent invasion.

Key words: angiogenesis, annexin A2, glioma, invasion, proteomics

INTRODUCTION

Gliomas are highly invasive and tend to diffusely infiltrate the brain, thereby placing tumor cells outside the margins of therapeutic resection. The mechanisms of invasion by glioma cells have been addressed in different studies and experimental settings, yet there is a need for a novel panel of biomarkers that characterize each invasive phenotype. Moreover, invasive nests of tumor cells are associated with initiation of neovascular angiogenesis and disruption of the blood-brain barrier through release of vasomodulatory cytokines. Taken together, these factors contribute to the rapid invasion process that is beyond the confines of the typical radiologically identifiable tumor mass, resulting in the near universally high rate of tumor recurrence and ultimate death.

Little is known about the distinct biology of invasive gliomas *in situ,* but their diffuse invasion profile suggests the activation of genetic and cellular mechanisms that distinguish them from the cells inside the tumor's core. Systematic analysis of tumor cells with different biological behaviors may help to elucidate the nature of each tumor's invasion pattern. Currently, the proteomic approach has made it possible to characterize the global alterations that occur in cellular protein expression. This proteomics-based analysis promises new insights into the cellular mechanisms involved in tumor invasion and is likely to result in the discovery of novel diagnostic markers and new therapeutic targets.

In our previous study, detailed histopathological observations of human glioblastoma tissue revealed that there are at least two invasive and angiogenic phenotypes: one dependent on angiogenesis and the other independent of angiogenesis. Glioma cells migrate along dilated vessels in angiogenesis-dependent invasion, while infiltration of single glioma cells into the brain tissue is unrelated to the vasculature in angiogenesis-independent invasion.[1,2] Moreover, we established two glioma cell lines (J3T-1 and J3T-2) that showed different invasion phenotypes when implanted in rat brains.[1,2] J3T-1 cells form comparatively well-demarcated and highly angiogenic tumors, while J3T-2 cells form tumors with obscure margins via single-cell infiltration into the normal brain parenchyma. J3T-1 and J3T-2 cells show angiogenesis-dependent and independent invasive patterns, respectively, in rat brain tumor models; these patterns resemble those of human glioblastoma invasion.

In the present study, this pair of cell lines was examined using a proteomics approach, including the use of two-dimensional gel electrophoresis (2DGE) and liquid chromatography-tandem mass spectrometry analysis (LC-MS/MS), to compare the proteomic profiles of these two cell lines with different invasion phenotypes.

MATERIALS AND METHODS

Cell Culture

The J3T canine glioma cell was a generous gift from Michael E. Berens MD, PhD (Translation Genomics Research Institute, Phoenix, AZ, USA).[3] Two cell lines—J3T-1 and J3T-2—were developed from the parental J3T cell line, as previously described.[1,4] In brief, J3T cells (5×10^6 cells) were subcutaneously implanted into the flanks of two athymic mice (NCr/Sed, nu/nu, 20 g). After 6 weeks, two tumors were established in each animal. These tumors were harvested in a sterile fashion, minced with a scalpel into 1-mm^3 cubes, treated for 1 h with 1 mg/ml Collagenase/Dispase (Roche, Basel, Switzerland), and subsequently cultured in Dulbecco's modified Eagle's medium (DMEM) supplemented with 10% fetal bovine serum (FBS), 100 units penicillin, and 0.1 mg streptomycin per milliliter. Both cell lines were derived from single subcutaneous tumors.

For enhanced visualization of J3T-1 and J3T-2 cells, cell lines were established that stably expressed green fluorescent protein (GFP), as previously described.[1] In brief, J3T-1 and J3T-2 cells were transfected with the pAcGFP1-C1 plasmid (Clontech Laboratories Inc, Mountain View, CA, USA), which encodes for GFP using the TransIT-LT1 reagent (Takara Bio Inc, Otsu, Japan) to obtain J3T-1G and J3T-2G, respectively. Cells were cultured in DMEM supplemented with 10% FBS, 100 units penicillin, and 0.1 mg streptomycin per milliliter in a standard tissue incubator at 37°C with a 5% CO_2 atmosphere.

2DGE

The cells were washed with a solution of phosphate-buffered saline (PBS) that contained 0.27% $CaCl_2 \cdot H_2O$, 0.02% $MgCl_2 \cdot 6H_2O$, 1% FBS, and 5 mM sodium pyruvate. Cells were harvested by mechanical scraping during the exponential growth phase. Cells were then centrifuged, and the cell pellets were dissolved in a lysis buffer that consisted of 5 M urea, 2 M thiourea, 2% 3-(3-cholamidopropyl)dimethylammonio-1-propane sulfonate (CHAPS), 2% sulfobetaine 3-10 (SB3-10), 1% dithiothreitol (DTT), and a protease inhibitor cocktail (Sigma-Aldrich, St. Louis, MO, USA). After three freeze-thaw cycles, the cell pellets were sonicated for 30 s and ultracentrifuged at 75,000 ×*g* for 30 min at 10°C using the Optima™ TLX ultracentrifuge (Beckman Coulter, Brea, CA, USA). The supernatant was transferred to a new tube and treated with ReadyPrep 2D Cleanup Kit (Bio-Rad, Hercules, CA, USA) to remove any ions, DNA, RNA, etc. The protein concentration was estimated using the RC-DC Protein Assay kit (Bio-Rad) according to manufacturer with two-washed standard protocol. For isoelectric focusing (IEF), Carrier ampholyte 5/8 (Bio-Rad) was formulated to increase the resolution at the basic end of the flatbed isoelectric focusing gel.

The first-dimensional IEF was performed using a 17-cm immobilized nonlinear pH gradient (5-8) strip (DryStrip; Bio-Rad). After rehydration for 15 h in a 300-µl buffer that consisted of 5M urea, 2M thiourea, 2% CHAPS, 3% SB3-10, 1% DTT, and 0.2% Bio-Lyte® 5/8 ampholyte (Bio-Rad), 60-µg samples of each protein were loaded onto the strips. Focusing was performed in

following step; (I) 250 V with linear increase for 40 min, (II)10000 V with linear increase for 4 h and (III) 10000 V with rapid increase for 7 h (total 70000V-hr); the samples were then maintained at 500 V, as needed.

The focused strips were then equilibrated in buffer I (6 M urea, 2% sodium dodecyl sulfate (SDS), 0.375 M Tris-HCl, 20% glycerol, and 2% DTT; pH 8.8) for 30 min and then buffer II (6 M urea, 2% SDS, 0.375 M Tris-HCl, 20% glycerol, and 2.5% iodoacetamide; pH 8.8) for 15 min with gentle shaking. The second-dimensional separation was carried out on 12% SDS-polyacrylamide gels using PROTEAN II Cell (Bio-Rad) at 20°C and 40 mA/gel for 4 h.

After 2DGE, the gels were stained with SYPRO Ruby (Invitrogen, Carlsbad, CA, USA) and Dodeca Silver Stain Kits (Bio-Rad), according to the manufacturer's protocol. Each experiment was performed in triplicate.

Image Analysis of 2DGE Gels

Images of the SYPRO Ruby-stained gels were obtained using a FLA-3000 image analyzer (Fujifilm, Tokyo, Japan). The images were analyzed using PDQuest Advanced, version 8.0 (Bio-Rad); analysis included background subtraction, spot detection, and volume normalization. The intensity of each spot was quantified by calculating the spot volume after normalization to the local regression model. The intensities of three sets of matched spots of each J3T-1 and J3T-2 gel were

compared, and a threshold ratio of 1.5 was used to screen for differences. Visual inspection confirmed the differences indicated by PDQuest analysis.

Protein Identification

The selected protein spots were manually excised from the gels after visualizing the spots with silver staining. After destaining and drying the excised spots, in-gel trypsin digestion using the Protein In-Gel Tryptic Digestion kit (Agilent Technologies, Santa Clara, CA, USA) was performed overnight at 30°C. The obtained peptide digests were analyzed using a fully automated nanoflow liquid chromatography-ion trap-tandem mass spectrometer (nLC-IT-MS/MS; Agilent 1100 LC/MSD Trap XCT Ultra, Agilent Technologies).

Protein identification was performed using the Spectrum Mill MS Proteomics Workbench platform (version A.03.02; Agilent Technologies), according to the workflow parameters specified by the manufacturer. The identification parameters were set as follows: database, NCBInr; species, Canis familialis; enzyme, trypsin; monoisotopic masses used; precursor mass tolerance (peptide tolerance), ±2.5 Da; product mass tolerance (MS/MS tolerance), ±0.8; fixed modification, carbamidomethylation (cysteine); and variable modification, oxidation (methionine). Two missed cleavages with trypsin were allowed and the instrument's setting was specified as ''ESI ion trap''. The probability scores calculated by the software were used as the criteria for correct identification.

Quantitative reverse-transcription PCR (QRT-PCR)

Total RNA was isolated from cultured J3T-1 and J3T-2 cells using RNeasy® Mini Kit (QIAGEN, Valencia, CA, USA) and reverse-transcribed with oligo dT primers using SuperScript III First-Strand Synthesis System for RT-PCR (Invitrogen), according to manufacturer's instructions. Primers specific for each target gene were designed using Primer Express (Applied Biosystems, Foster City, CA, USA) and synthesized by Invitrogen. The resulting cDNA was amplified by PCR using gene-specific primers and the 7300 Real Time PCR system (Applied Biosystems) and QuantiTect™ SYBR® Green PCR kit (QIAGEN). A log-linear relationship between the amplification curve and quantity of cDNA in the range of 1 to 1000 copies was observed.

The cycle number at the threshold was used as the threshold cycle (Ct). The different expression of mRNA was deducted from $2^{-\Delta\Delta Ct}$ using the 7300 Real Time PCR System with the Sequence Detection software (version 1.4; Applied Biosystems). The amount of cDNA in each sample was normalized to the crossing point of the housekeeping gene *GAPDH*. The following thermal cycling parameters were used: denaturation at 95°C for 15 min, followed by 40 cycles of 30 s at 94°C, 30 s at 55°C, and 1 min at 72°C. The relative mRNA upregulation for each gene in the J3T-2 cells was calculated using their respective crossing points in the following formula:

$$F=2^{(TH-TG)-(OH-OG)}$$

where, F = fold difference, T = J3T-2 cells, O = J3T-1 cells,

H = housekeeping gene (*GAPGH*), and G = gene of interest.

Immunohistochemistry

All experimental animals were housed and handled in accordance with the Okayama University Animal Research Committee guidelines. Before implantation, 85–90% of the confluent J3T-1, J3T-2, J3T-1G, and J3T-2G cells were trypsinized, rinsed with a solution of DMEM and 10% FBS, and centrifuged at 800 rpm for 5 min. The resulting pellets were resuspended in PBS and the concentration was adjusted to 1×10^5 cells/μl of PBS. To establish the brain tumor models, athymic rats (F344/N-nu/nu; CLEA Japan, Inc., Tokyo, Japan) were anesthetized with an intraperitoneal injection of nembutal (30 mg/kg) and placed in a stereotactic apparatus (Narishige, Tokyo, Japan). Tumor cells (5×10^5 cells/5 μl) were slowly injected into the basal ganglia of the right cerebral hemisphere (4 mm lateral and 1 mm anterior to the bregma at a depth of 4 mm) using a Hamilton syringe (Hamilton, Reno, NV, USA), according to previously published procedures.[1,5] For histological examination, the athymic rats (J3T-1, n = 5; J3T-2, n = 5) were sacrificed 4–5 weeks after tumor inoculation. Before sacrifice, the animals were anesthetized. Death was induced via cardiac puncture, then the animals were perfused with 100 ml PBS and fixated with 200 ml of 4% paraformaldehyde. The brains were removed and stored in 4% paraformaldehyde for at least 24 h.

Snap-frozen tissue samples were embedded in an optimal cutting temperature compound for cryosectioning. Sixteen-micrometer cryostat sections were processed for indirect immunofluorescence analysis. The slides were incubated with 10% horse serum in PBS at room temperature and then with the anti-annexin A2 antibody (1:20 mouse IgG; Zymed Laboratories, San Francisco, CA, USA) diluted with 1% horse serum in PBS, and stored overnight at 4°C. After three washes with PBS for 5 min, the slides were incubated with Cy3-conjugated antibodies against mouse IgG (1:300) (Jackson ImmunoResearch Laboratories, Inc., West Grove, PA, USA) and 4′, 6-diamino-2-phenylindole in PBS (1:500; Invitrogen) for 60 min. The slides were then washed with PBS and mounted.

Human glioma samples were intraoperatively obtained from patients undergoing surgical removal of tumors for diagnostic and therapeutic purposes (Okayama University Hospital, Okayama, Japan). Written informed consent was taken in all the cases before surgery. Lobectomies were performed to remove the entire tumor and any surrounding brain parenchyma beyond the boundaries of the tumors observed on MRI. All glioma specimens were diagnosed and graded according to the World Health Organization classification of tumors of the central nervous system, and all five specimens were diagnosed as glioblastomas. No patient had received radiation or chemotherapy before surgery.

After deparaffinization in xylene and rehydration in decreasing concentrations of ethanol,

4-μm-thick sections were incubated in 0.3% hydrogen peroxide (30 min) and autoclaved with distilled water for 10 min at 121°C. After three washes in PBS, the sections were incubated with anti-annexin A2 monoclonal antibodies (1:20) (mouse IgG; Zymed Laboratories) that had been diluted with PBS and 5% skim milk (60 min) at room temperature. Secondary antibody was applied using the DakoCytomation Envision^{+} System-HRP kit, according to the manufacturer's protocol (DakoCytomation, Carpinteria, CA, USA). The sections were visualized using 3,3'-Diaminobenzidine (DAB).

Annexin A2 expression was qualitatively scored as follows: (-) for no staining (nearly 0% of cells were labeled), (+) for a trace of positive cells (less than 30% of cells were labeled), (++) for moderately diffuse staining or sparsely intensive staining (30%–60% of cells were labeled, and less than 30% of cells were labeled with the strong intensity), and (+++) for strongly diffuse staining (60%–100% of cells were labeled). T.M. and S.I. classified the tumors according to 3 representative fields without prior knowledge of the patients' clinical or radiological data.

RESULTS

2DGE patterns and differential analysis of J3T-1 and J3T-2

The 2DGE gel images of J3T-1 and J3T-2 cells showed similar protein expression patterns, probably reflecting the genetic similarity of J3T-1 and J3T-2 **(Fig. 1)**.

Using the PDQuest 2DGE gel analysis software, approximately 2800 well-stained and clearly delineated protein spots were detected. Twenty-two spots showing more than 1.5-fold change in spot intensity; five of these protein spots were upregulated in J3T-1 and 17 were upregulated in J3T-2. These differentially expressed protein spots are illustrated with circles and spot numbers in Fig. 1A and 1B.

Proteins identified by LC-MS/MS

Differentially expressed protein spots were excised from the 2DGE gels and analyzed for protein identification by LC-MS/MS and database searching. As a result, 18 proteins were identified in those spots; these proteins are shown in Table 1. The Spectrum Mill software calculates the MS/MS Search score as described below. Each peak assigned to an allowed fragment ion type for a candidate peptide sequence is given "bonus points". In contrast, each unassigned peak is given "penalty points". Penalty value is based on peak height, - (peak height / height of tallest peak). MS/MS score is summation of these bonus points and penalty points, indicating probability of the protein. Thus, the higher score indicates the better probability. The identified proteins that were upregulated in J3T-1 included one metabolic enzyme, one storage protein, one structural protein, and one phospholipid-binding protein. Proteins that were upregulated in J3T-2 included eight metabolic enzymes, two translational regulatory proteins, two RNA-binding proteins, one GTP-binding protein,

and one signal transduction protein. Metabolic enzymes constituted more than half of the proteins that were upregulated in J3T-2.

Fig. 2A and 2B shows the distribution of all the 18 identified proteins that were upregulated in J3T-1 and J3T-2 according to their general functions as described in NCBI Entrez Gene Database (http://www.ncbi.nlm.nih.gov/sites/entrez?db=gene) and Human Protein Reference Database (http://www.hprd.org/index_html). Fig. 2C shows the representative MS/MS spectrum for the peptide sequence matched to annexin A2 identified from spot No.4.

Candidate protein validation by QRT-PCR

A summary of the QRT-PCR data is shown in Fig. 3. Similar patterns were observed for the gene expression profiles obtained with the proteomics and QRT-PCR data. The directionality of expression of 17 of the 18 genes coincided with the expression of the corresponding proteins. Fourteen of 18 genes demonstrated more than 1.5-fold change in expression (as denoted by the asterisks [*] in Fig. 3), while the rest of the proteins did not show marked difference in expression between J3T-1 and J3T-2 cells.

Immunohistochemical corroboration of candidate proteins observed in the invasive animal models

Representative photomicrographs of the invasive animal models are presented in Fig. 4A, B. J3T-1 cells formed well-demarcated and highly angiogenic tumors. In contrast, J3T-2 cells formed tumors with obscure margins via single-cell infiltration into the normal brain parenchyma.

The results of this proteomics-based analysis of the proteins involved in invasion were corroborated by immunohistochemical analysis of the J3T-1G and J3T-2G xenograft models. One of the identified proteins was annexin A2, which has been reported to be involved in tumor invasion and metastasis.[6-8] Therefore, this protein was further studied using both animal models and human glioma samples. The annexin A2 antibody was readily available for immunohistochemical analysis of the frozen sections. Intense staining of the annexin A2 protein in the cytoplasm of the J3T-1 tumor cells was observed, whereas almost no staining was observed in the J3T-2 tumor cells **(Fig. 4 C-H)**, as expected based on the results of the proteomic analysis.

Immunohistochemical analysis of annexin A2 in human glioma samples

To analyze expression pattern of annexin A2 in relation to vasculature, immunohistochemical staining with anti-annexin A2 antibody was performed in 5 human glioblastoma samples. Patient's age, sex, tumor locations, and degree of annexin A2 expression are summarized in Table 2. The center of the tumor comprised an area of high-density tumor cells which were negative or weakly positive for annexin A2. Marked angiogenesis, which was characterized by

thick endothelial proliferation, was seen in the center and at the tumor borders. At the borders, clusters of annexin A2-positive tumor cells were observed around dilated vessels in all cases (**Fig. 5A**). Furthermore, diffuse single cell infiltration from the tumor core to the surrounding normal brain parenchyma, which was independent of vascular structure, was observed. Those cells were mostly negative (four cases) or weakly positive (one case; Patient 3) for annexin A2 (**Fig. 5B**).

DISCUSSION

To investigate the molecular basis of the invasive properties of malignant gliomas, proteomic analysis of the invasion-related proteins was performed using two unique sibling glioma cell lines, J3T-1 and J3T-2, which exhibit different aspects of human glioma invasion *in situ.*

Advantages of the proteomic method for identifying invasion-related proteins

This study describes how four proteins were observed in J3T-1 cells and 14 proteins were observed in J3T-2 cells, out of 2800 protein spots that were reproducibly identified on 2DGE gels at pH 5-8.

The similarities in the protein expression patterns on the 2DGE gel images of J3T-1 and J3T-2 cells reflect their genetic proximity. At the same time, significant differences in protein expression between these two cell lines do exist, which could be directly related to their invasive

characteristics. Taken together, the proteomic method could be used to sensitively capture the features of the cell lines used in this study.

The results of these proteomic analyses were corroborated by the results of the QRT-PCR and immunohistochemical analyses. Nearly all proteins that were shown to be upregulated by the 2DGE method were also upregulated at the mRNA level. This method is simple, reproducible, and reliable and may prove useful for gaining a broader understanding of invasion in general as well as some of the advantages and pitfalls of other *in vitro* modeling systems.

As a shortcoming, 2DGE analysis usually cannot detect hydrophobic membrane proteins, proteins larger than 100 kDa, low-abundance proteins,[9] or proteins with pI values outside the pH range.[10] These limitations of standard 2DGE probably account for the less chance of this study to identify these types of proteins in J3T-1 and J3T-2 cells.

Advantages of the two subclones for proteomic analysis

There are several advantages in using invasive animal models and proteomic analysis to study the molecular basis of glioma invasion.

First, the animal models used in this study are one of the few models available for studying invasive glioma in experimental settings.[1,2] Traditional animal glioma models do not exhibit invasive growth into the surrounding normal brain areas and have been criticized for not recapitulating the

main pathological features of human glioma.[11] Recently, several experimental glioma models showing varying degrees of invasion have been developed to study glioma cell invasion both *in vitro* and *in vivo*.[12,13]

Second, the two subclones that were established from the same parental cell line showed very different invasive phenotypes when inoculated in rat brains; however, the subclones have inherently similar genetic backgrounds.[4] These differences in phenotypes are supposed to arise from differences in genotype. This allowed for direct comparison of the differentially expressed proteins that characterize the phenotypic differences in their invasive capabilities.

Third, the animal models used in this study are reproducible and suitable for *in vivo* experiments. Therefore, candidate proteins that might affect the invasive capability of the tumor can be directly verified *in vivo* using these animal models.

Annexin A2 as a candidate invasion-related protein

One of the proteins identified, annexin A2, was expressed at higher levels in J3T-1 cells than in J3T-2 cells. Annexin A2 has been previously reported to be expressed on the tumor cell surface and to be involved in tumor invasion and metastasis.[6-8] Therefore, this protein's role in both animal models and human glioma samples was further examined.

Annexins are a superfamily of closely related calcium- and membrane-binding proteins

that are expressed in specific cell types. Annexins comprise numerous gene products, including 12 that are formed in vertebrates (group A annexins), and have been proposed to be involved in a variety of functions, including control of membrane structures, vesicle trafficking, cell division, apoptosis, calcium signaling, and growth regulation.[14-20] All annexins share a characteristic molecular structure that consists of a variable N-terminal domain and a highly conserved C-terminal domain, which is also called the annexin core. The core domain of annexin A2 harbors several Ca^{2+}-binding sites and one actin-binding domain, whereas the N-terminal domain contains the binding site for the cellular ligand S100A10 and a Ca^{2+}-independent membrane-binding domain. In cells, annexin A2 exists either as a monomer or as a heterotetrameric complex with S100A10.[21] Cell-surface annexin A2 has been shown to be a receptor/binding protein for both proteases (cathepsin B, plasminogen, and tissue-type plasminogen activator [tPA]) and extracellular matrix proteins (type I collagen and tenascin C) that are involved in tumor invasion and metastasis.[6-8] tPA has been shown to bind specifically to annexin A2 on the extracellular membrane of pancreatic cancer cells where it activates plasmin production and promotes tumor cell invasion. Annexin A2 is also expressed on the surface of vascular endothelial cells and has been shown to play a significant role in the regulation of tPA activities, plasminogen activation, and angiogenic functions.[22,23] Increased expression of annexin A2 has been described in several types of tumor, including gastric carcinoma,[24] colorectal cancer,[25] pancreatic cancer,[26] breast cancer,[27] high-grade gliomas,[28] kidney

cancer,[29] and vascular tumors.[30] In gliomas, annexin A2 has been identified more frequently in high-grade gliomas than in low grade gliomas[10] and is known to be an independent prognostic factor for poor clinical outcomes in patients with gliomas.[28,31] Because of the ability of annexin A2 to interact with the actin cytoskeleton[14,15,32] and tumor-released proteases,[15] annexin A2 has become a promising candidate for influencing the invasion processes of glioma cells. Recent proteomic investigations of the pseudopodia extensions of highly migratory U87MG glioma cells have reported increased levels of annexin A2.[33] Tatenhorst et al. demonstrated that the migration of human glioma cells is significantly inhibited following annexin A2 depletion by RNA interference techniques *in vitro.*[34] Moreover, cell-surface annexin A2 is a receptor for angiostatin, which is an internal fragment of plasminogen. Annexin A2-dependent localized plasmin generation could contribute to angiogenesis and metastasis. Therefore, by blocking annexin A2-dependent plasmin production, e.g., by using angiostatin, it may be possible to develop new anti-angiogenic therapies.[35]

A previous study reported that there are at least two invasive and angiogenic phenotypes—angiogenesis-dependent invasion and angiogenesis-independent invasion—and the novel animal glioma models used in this study were able to exhibit these phenotypes.[1,2] The histopathological features of angiogenesis-dependent invasion are characterized by robust neovascular formation in the normal parenchyma adjacent to the main tumor mass and the formation of clusters of glioma cells. In contrast, angiogenesis-independent invasion is characterized by the

formation of poorly demarcated tumors that show single-cell infiltrations into the surrounding normal brain tissue without angiogenic activities.

In the present study, annexin A2 was upregulated in J3T-1 cells, which typically show angiogenesis-dependent invasion in rat brain. In addition, immunohistochemical analysis of human glioblastoma samples revealed that annexin A2 is expressed in clusters of tumor cells around dilated vessels located at the border of the tumor, suggesting that annexin A2 has a functional role in angiogenesis-dependent invasion. The authors consider that neo-angiogenesis is an important factor that contributes to the regulation of invasion patterns. Recent studies have shown that glioma cell lines derived from transgenic mice that lack VEGF expression form tumors with irregular borders and are highly invasive along blood vessels, as compared with the sharp borders seen in tumors derived from the glioma cells that have been transfected to overexpress VEGF.[36] This observation is consistent with the result of the present study, suggesting that annexin A2 plays a key role in angiogenesis-dependent invasion by interacting with VEGF and other proangiogenic factors. With regard to the relationship between annexin A2 and VEGF, Zhao et al. demonstrated that the increased expression of annexin A2 in ischemic retinas is induced by increased levels of VEGF mRNA. Zhao et al. concluded that annexin A2 is a functional protein in VEGF expression in retinal neovascularization and is induced by hypoxia.[37]

Additional findings

Other noticeable proteins expressed higher in J3T-2 are heterogeneous nuclear ribonucleoproteins (hnRNPs) and Septin 11.

hnRNPs comprise a large family of proteins, including approximately 30 members that share some structural domains. The results obtained in our study show HNRNPK and HNRNPA1 are up-regulated in J3T-2. hnRNPs play important roles in telomere biogenesis, DNA repair, cellular signaling, and the regulation of expression at both the transcriptional and translational levels.[38] In addition, the nuclear shift of HNRNPK in dividing cells suggests a role in proliferating cells.[39] So far, there have been no detailed reports about functions of hnRNPs in gliomas.

Septins are a highly conserved subfamily of GTPases that play an important role in maintaining cytoskeletal structures necessary for the control of cell division, and are required for cytokinesis.[40] Kim et al. showed that septins are variably expressed in human brain tumor cell lines and specimens using antibodies against septins 2, 3, 4, 5, 6, 7, 9, and 11 in immunofluorescence and Western blot analysis.[41] In their study, septin 11 was immunolocalized along with the actin microfilamentous system, suggesting possible involvement in cell motility function.

These proteins are not fully investigated in terms of their function in glioma invasion and await further study.

CONCLUSION

Proteomic methods were used to compare the protein profiles of two cell lines with different invasive characteristics. This comparative analysis revealed the differential expression of several proteins that may be involved in tumor cell invasion. Among them, annexin A2 was shown to be one of the candidate proteins which are involved in angiogenesis-dependent invasion.

This study will help to elucidate the mechanisms involved in glioma cell invasion and will aid in the selection of targets for the molecular treatment of malignant gliomas.

Acknowledgements

This study was supported by grants-in-aid for Scientific Research from the Japanese Ministry of Education, Culture, Sports, Science, and Technology to T.I. (No. 19591675), H.K. (No. 19591676), and K.K. (No. 20890133; No. 21791364), and Okayama University Budget for Centers of Excellence. We thank H. Wakimoto, M. Arao, and A. Ishikawa for their technical assistance. Following medical students also contributed animal experiments: T. Oka, K. Tanaka, H. Honda, K. Seno, H. Okura, T. Mifune, and S. Murai.

References

1. Inoue S, Ichikawa T, Kurozumi, K, et al. Novel animal glioma models that separately exhibit two different invasive and angiogenic phenotypes of human glioblastomas. *World Neurosurg* 2011. doi: 10.1016/j.wneu.2011.09.005

2. Onishi M, Ichikawa T, Kurozumi K, Date I. Angiogenesis and invasion in glioma. *Brain Tumor Pathol* 2011;28:13-24.

3. Berens ME, Bjotvedt G, Levesque DC, Rief MD, Shapiro JR, Coons SW. Tumorigenic, invasive, karyotypic, and immunocytochemical characteristics of clonal cell lines derived from a spontaneous canine anaplastic astrocytoma. *In Vitro Cell Dev Biol Anim* 1993;29:310-318.

4. Hampl JA, Camp SM, Mydlarz WK, et al. Potentiated gene delivery to tumors using herpes simplex virus/Epstein-Barr virus/RV tribrid amplicon vectors. *Hum Gene Ther* 2003;14:611-626.

5. Ichikawa T, Tamiya T, Adachi Y, et al. In vivo efficacy and toxicity of 5-fluorocytosine/cytosine deaminase gene therapy for malignant gliomas mediated by adenovirus. *Cancer Gene Ther* 2000;7:74-82.

6. Mai J, Waisman DM, Sloane BF. Cell surface complex of cathepsin B/annexin II tetramer in malignant progression. *Biochim Biophys Acta* 2000;1477:215-230.

7. Díaz VM, Hurtado M, Thomson TM, Reventós J, Paciucci R. Specific interaction of tissue-type

plasminogen activator (t-PA) with annexin II on the membrane of pancreatic cancer cells activates plasminogen and promotes invasion in vitro. *Gut* 2004;53:993-1000.

8. Zhai H, Acharya S, Gravanis I, et al. Annexin A2 promotes glioma cell invasion and tumor progression. *J Neurosci* 2011;31(40):14346-14360.

9. Vogel TW, Zhuang Z, Li J, et al. Proteins and protein pattern differences between glioma cell lines and glioblastoma multiforme. *Clin Cancer Res* 2005;11:3624-3632.

10. Iwadate Y, Sakaida T, Hiwasa T, et al. Molecular classification and survival prediction in human gliomas based on proteome analysis. *Cancer Res* 2004;64: 2496-2501.

11. de Vries NA, Beijnen JH, van Tellingen O. High-grade glioma mouse models and their applicability for preclinical testing. *Cancer Treat Rev* 2009;35:714-723.

12. Martens T, Laabs Y, Günther HS, et al. Inhibition of glioblastoma growth in a highly invasive nude mouse model can be achieved by targeting epidermal growth factor receptor but not vascular endothelial growth factor receptor-2. *Clin Cancer Res* 2008;14:5447-5458.

13. Giannini C, Sarkaria JN, Saito A, et al. Patient tumor EGFR and PDGFRA gene amplifications retained in an invasive intracranial xenograft model of glioblastoma multiforme. *Neuro Oncol* 2005;7:164-176.

14. Rescher U, Gerke V. Annexins--unique membrane binding proteins with diverse functions. *J Cell Sci* 2004;117:2631-2639.

15. Gerke V, Moss SE. Annexins: from structure to function. *Physiol Rev* 2002;82:331-371.

16. Gerke V, Creutz CE, Moss SE. Annexins: linking Ca2+ signalling to membrane dynamics. *Nat Rev Mol Cell Biol* 2005;6:449-461.

17. Hayes MJ, Moss SE. Annexins and disease. *Biochem Biophys Res Commun* 2004;322:1166-1170.

18. Hayes MJ, Longbottom RE, Evans MA, Moss SE. Annexinopathies. *Subcell Biochem* 2007;45:1-28.

19. Rand JH. The annexinopathies: a new category of diseases. *Biochim Biophys Acta* 2000;1498:169-173.

20. Mussunoor S, Murray GI. The role of annexins in tumour development and progression. *J Pathol* 2008;216:131-140.

21. Zobiack N, Gerke V, Rescher U. Complex formation and submembranous localization of annexin 2 and S100A10 in live HepG2 cells. *FEBS Lett* 2001;500:137-140.

22. Ling Q, Jacovina AT, Deora A, et al. Annexin II regulates fibrin homeostasis and neoangiogenesis in vivo. *J Clin Invest* 2004;113:38-48.

23. Hajjar KA, Jacovina AT, Chacko J. An endothelial cell receptor for plasminogen/tissue plasminogen activator. I. Identity with annexin II. *J Biol Chem* 1994;269:21191-21197.

24. Emoto K, Sawada H, Yamada Y, et al. Annexin II overexpression is correlated with poor

prognosis in human gastric carcinoma. *Anticancer Res* 2001;21:1339-1345.

25. Duncan R, Carpenter B, Main LC, Telfer C, Murray GI. Characterization and protein expression profiling of annexins in colorectal cancer. *Br J Cancer* 2008;98:426-433.

26. Esposito I, Penzel R, Chaib-Harrireche M, et al. Tenascin C and annexin II expression in the process of pancreatic carcinogenesis. *J Pathol* 2006;208:673-685.

27. Sharma MR, Koltowski L, Ownbey RT, Tuszynski GP, Sharma MC. Angiogenesis-associated protein annexin II in breast cancer: selective expression in invasive breast cancer and contribution to tumor invasion and progression. *Exp Mol Pathol* 2006;81:146-156.

28. Reeves SA, Chavez-Kappel C, Davis R, Rosenblum M, Israel MA. Developmental regulation of annexin II (Lipocortin 2) in human brain and expression in high grade glioma. *Cancer Res* 1992;52:6871-6876.

29. Zimmermann U, Woenckhaus C, Pietschmann S, et al. Expression of annexin II in conventional renal cell carcinoma is correlated with Fuhrman grade and clinical outcome. *Virchows Arch* 2004;445:368-374.

30. Syed SP, Martin AM, Haupt HM, Arenas-Elliot CP, Brooks JJ. Angiostatin receptor annexin II in vascular tumors including angiosarcoma. *Hum Pathol* 2007;38:508-513.

31. Siao CJ, Tsirka SE. Tissue plasminogen activator mediates microglial activation via its finger domain through annexin II. *J Neurosci* 2002;22:3352-3358.

32. Hayes MJ, Rescher U, Gerke V, Moss SE. Annexin-actin interactions. *Traffic* 2004;5:571-576.

33. Beckner ME, Chen X, An J, Day BW, Pollack IF. Proteomic characterization of harvested pseudopodia with differential gel electrophoresis and specific antibodies. *Lab Invest* 2005;85:316-327.

34. Tatenhorst L, Rescher U, Gerke V, Paulus W. Knockdown of annexin 2 decreases migration of human glioma cells in vitro. *Neuropathol Appl Neurobiol* 2006;32:271-277.

35. Sharma MC, Sharma M. The role of annexin II in angiogenesis and tumor progression: a potential therapeutic target. *Curr Pharm Des* 2007;13:3568-3575.

36. Pàez-Ribes M, Allen E, Hudock J, et al. Antiangiogenic therapy elicits malignant progression of tumors to increased local invasion and distant metastasis. *Cancer Cell* 2009;15:220-231.

37. Zhao S, Huang L, Wu J, Zhang Y, Pan D, Liu X. Vascular endothelial growth factor upregulates expression of annexin A2 in vitro and in a mouse model of ischemic retinopathy. *Mol Vis* 2009;15:1231-1242.

38. Carpenter B, MacKay C, Alnabulsi A, et al. The roles of heterogeneous nuclear ribonucleoproteins in tumour development and progression. *Biochim Biophys Acta* 2006;1765(2):85-100.

39. Ostrowski J, Bomsztyk K. Nuclear shift of hnRNP K protein in neoplasms and other states of enhanced cell proliferation. *Br J Cancer* 2003;89(8):1493-1501.

40. Kinoshita M, Kumar S, Mizoguchi A, et al. Nedd5, a mammalian septin, is a novel cytoskeletal component interacting with actin-based structures. *Genes Dev* 1997;11(12):1535-1547.

41. Kim DS, Hubbard SL, Peraud A, Salhia B, Sakai K, Rutka JT. Analysis of mammalian septin expression in human malignant brain tumors. *Neoplasia* 2004;6(2):168-178.

Figure Legends

Fig.1 SYPRO Ruby-stained two-dimensional gel electrophoresis (2DGE) gel images of J3T-1 (A) and J3T-2 (B) cells. The arabic numbers indicate the differentially expressed spots; the numbers refer to those reported in Table 1. The protein expression levels of spots 1–5 were upregulated in J3T-1 cells. The protein expression levels of spots 6–22 were upregulated in J3T-2 cells. pI, isoelectric point; MW, molecular weight; Da, Daltons.

Fig.2 Distribution of proteins according to their function and representative MS/MS spectrum. A and B: Pie charts representing the distribution of the identified proteins according to their general functions. Assignments were made on the basis of information provided from the NCBI Entrez Gene and Human Protein Reference Database. A: Upregulated proteins in J3T-1 cells. B: Upregulated proteins in J3T-2 cells. C: The representative MS/MS spectrum for the peptide sequence matched to annexin A2.

Fig.3 Quantitative reverse-transcription PCR (QRT-PCR) validation of candidate proteins shown to be differentially expressed in J3T-1 and J3T-2 cells by proteomic analysis. The names of the analyzed transcripts are listed along the x-axis and the fold-change increases of each gene in J3T-1 vs J3T-2 cells (i.e., differences in the relative copy numbers, where 1 represents equal expression

levels in both populations) are listed along the y-axis. Asterisks denote genes that demonstrated more than 1.5-fold change in expression levels.

Fig.4 *In vivo* analysis of the invasive animal model. Macroscopic and microscopic appearance of two distinct invasion phenotypes in athymic rats harboring J3T-1 (A) and J3T-2 (B) brain tumors are shown. J3T-1 cells form well-demarcated and highly angiogenic tumors. Multiple small satellite tumors are also observed at the tumor borders. J3T-2 cells gradually dispersed from the tumor center to the surrounding normal brain tissue. All sections are stained with hematoxylin-eosin. Bars indicate 300 μm. Immunohistochemical analysis of annexin A2 was performed using rat brain samples that harbored green fluorescent protein (GFP)-expressing J3T-1 (C, D, E) and J3T-2 (F, G, H) brain tumors. The annexin A2 antibody was visualized using the Cy3-conjugated secondary antibody (red). The remarkable staining of annexin A2 in the cytoplasm of J3T-1 tumor cells is shown (D, E); J3T-2 tumor cells were hardly stained by the same antibody (G, H).

Fig.5 Results of immunohistochemical analysis of annexin A2 in human glioma samples. Representative photomicrographs of paraffin-embedded sections of glioblastomas from patient 2, which were immunostained for annexin A2. Cells clustering around the dilated vessels located at the border of the tumor are moderately positive for annexin A2 (A). Tumor cells migrating from the

tumor center into normal brain parenchyma were mostly negative or very weakly positive for annexin A2 (B). Magnification, ×100. Scale bar = 200μm.

Fig. 1

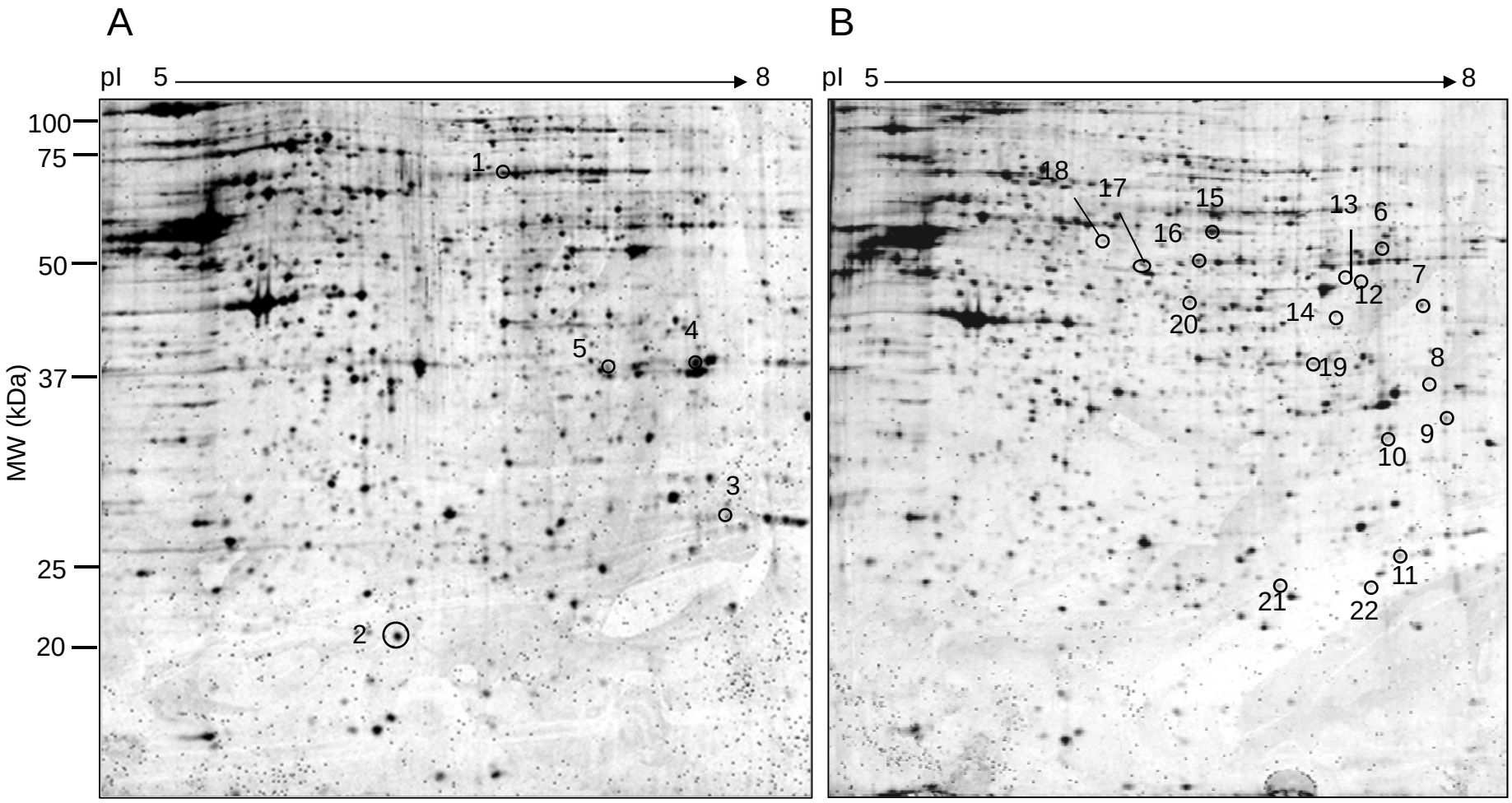
A
pI 5
8
100
75
50
37
25
20
MW (kDa)
1
2
3
4
5
B
pI 5
8
18
17
15
13
6
16
7
12
20
14
8
19
9
10
11
21
22

Fig. 2

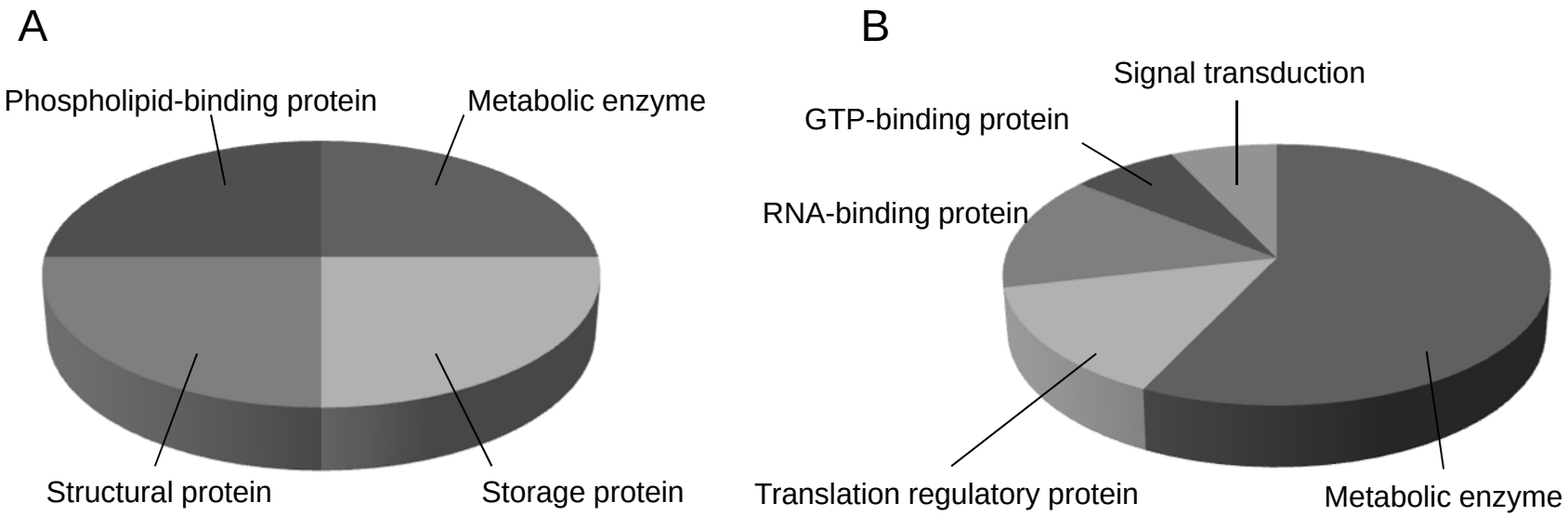
A
Phospholipid-binding protein
Metabolic enzyme
Structural protein
Storage protein
B
Signal transduction
GTP-binding protein
RNA-binding protein
Translation regulatory protein
Metabolic enzyme

C

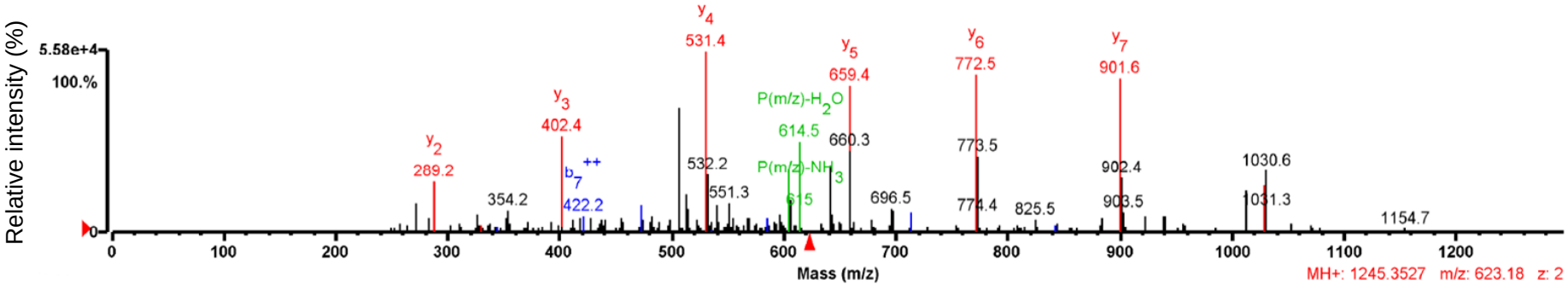
Relative intensity (%)
5.58e+4
100.%
0
y2
289.2
y3
402.4
b7++
422.2
354.2
y4
531.4
532.2
551.3
y5
659.4
P(m/z)-H2O
614.5
P(m/z)-NH3
615
660.3
696.5
y6
772.5
773.5
774.4
825.5
y7
901.6
902.4
903.5
1030.6
1031.3
1154.7
0
100
200
300
400
500
600
700
800
900
1000
1100
1200
Mass (m/z)
MH+: 1245.3527 m/z: 623.18 z: 2

Fig. 3

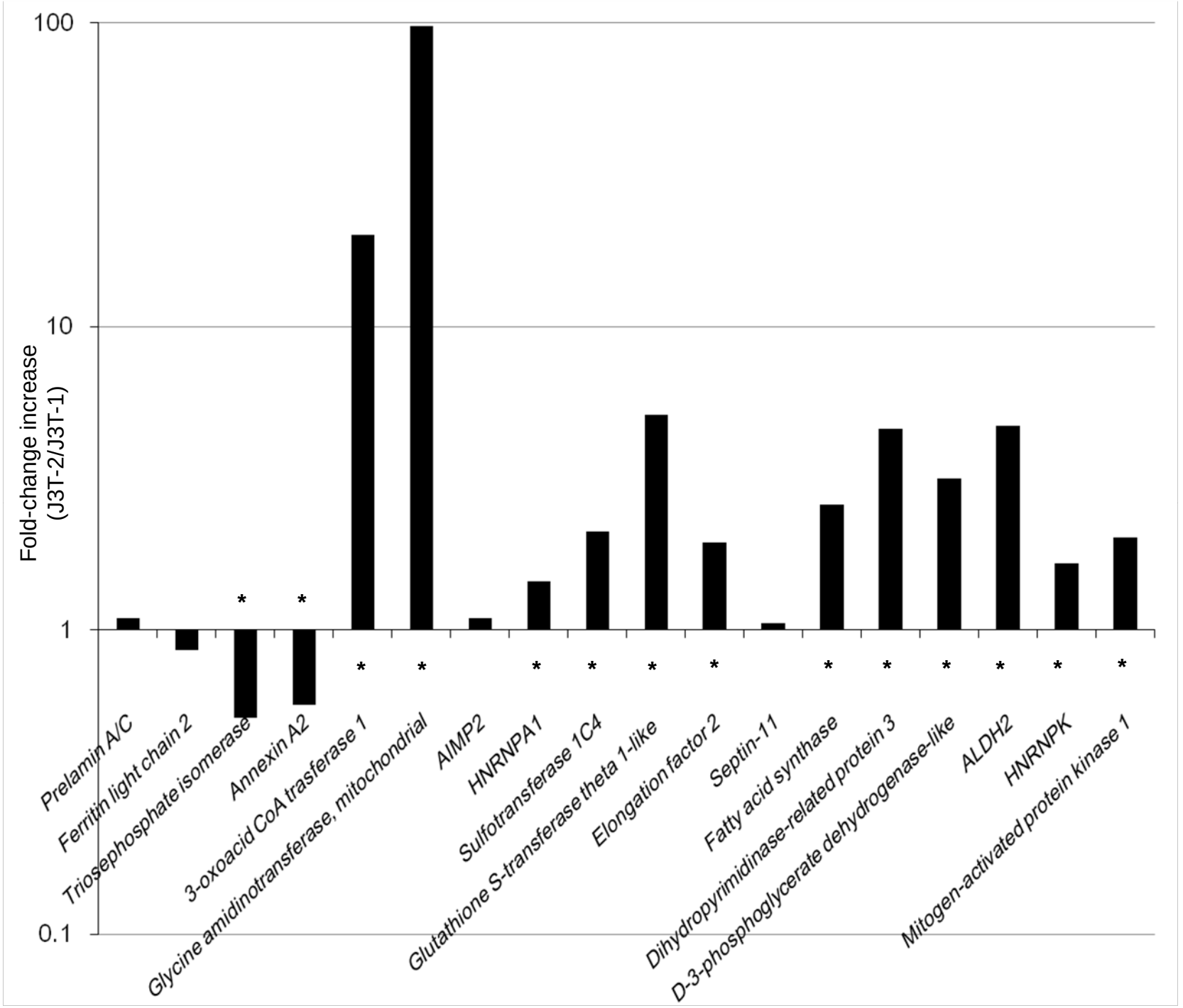
100
10
1
0.1
Fold-change increase
(J3T-2/J3T-1)
*
*
*
*
*
*
*
*
*
*
*
*
*
*
Prelamin A/C
Ferritin light chain 2
Triosephosphate isomerase
Annexin A2
3-oxoacid CoA trasferase 1
Glycine amidinotransferase, mitochondrial
AIMP2
HNRNPA1
Sulfotransferase 1C4
Glutathione S-transferase theta 1-like
Elongation factor 2
Septin-11
Fatty acid synthase
Dihydropyrimidinase-related protein 3
D-3-phosphoglycerate dehydrogenase-like
ALDH2
HNRNPK
Mitogen-activated protein kinase 1

Fig. 4

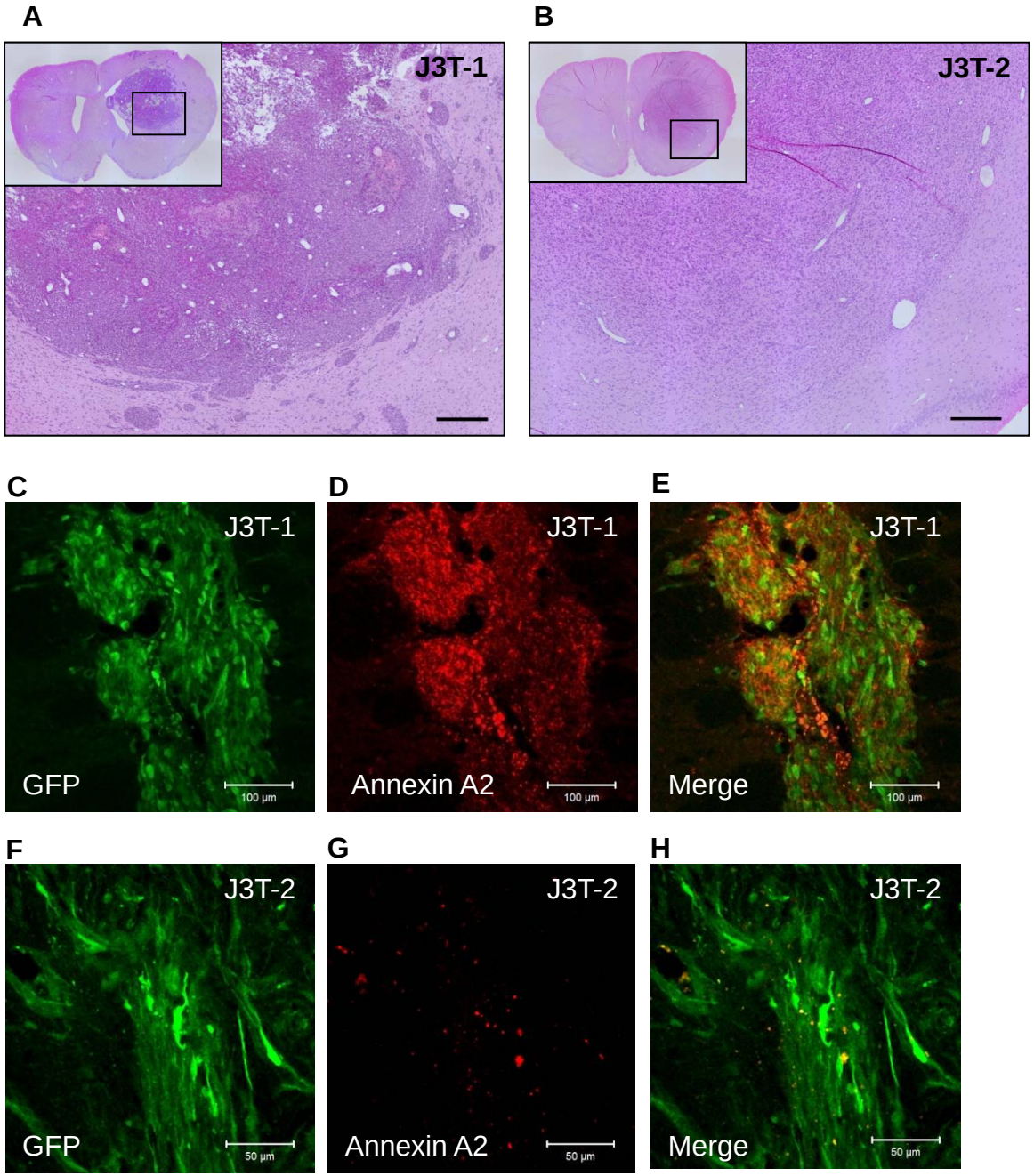
A
J3T-1
B
J3T-2
C
J3T-1
GFP
100 μm
D
J3T-1
Annexin A2
100 μm
E
J3T-1
Merge
100 μm
F
J3T-2
GFP
50 μm
G
J3T-2
Annexin A2
50 μm
H
J3T-2
Merge
50 μm

Fig. 5

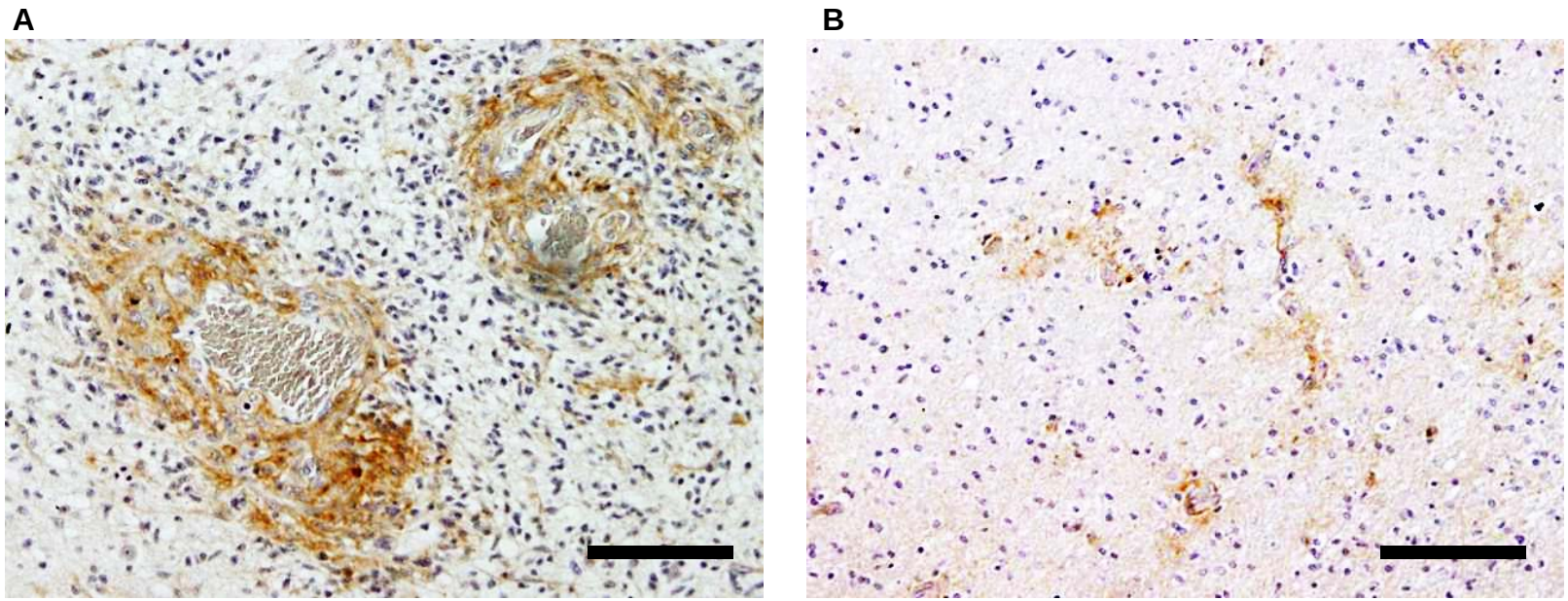

Table 1 Results of differentially expressed proteins in J3T-1 and J3T-2 cells

Spot No.†	Protein name	NCBI-AC‡	MW(Da)/pI	AA§(%)	MS/MS score	Potential biological function
Up-regulated in J3T-1						
1	Prelamin A/C isoform4	XP_864434	74226/6.57	40	408.01	Structural protein components of the nuclear lamina
2	Ferritin light chain 2	XP_536874	28397.3/5.39	14	55.69	Storage protein (iron ion transport)
3	Triosephosphate isomerase	NP_001183983	26714.7/6.9	28	82.69	Metabolic enzyme (fatty acid biosynthesis, gluconeogenesis, glycolysis)
4	Annexin A2	NP_001002961	38654.3/6.92	6	26	Calcium-dependent phospholipid-binding protein, regulation of cellular growth and in signal transduction pathways
5	Not identified					

Up-regulated in J3T-2

6	3-oxoacid CoA transferase 1	XP_536487	64746/7.91	12	103.21	Metabolic enzyme (ketone body catabolism)
7	Glycine amidinotransferase, mitochondrial	XP_544663	48379.7/8.59	21	119.73	Metabolic enzyme (creatine biosynthesis)
8	Aminoacyl tRNA synthase complex-interacting multifunctional protein 2-like (AIMP2)	XP_536880	35298.8/7.07	12	37.41	Translation regulatory protein, protein metabolism
9	Heterogeneous nuclear ribonucleoprotein A1 (HNRNPA1)	XP_851182	42254.5/9.27	6	29	RNA-binding protein (Regulation of nucleobase, nucleoside, nucleotide and nucleic acid metabolism)
10	Sulfotransferase 1C4	XP_531771	35461.8/6.87	10	40.15	Metabolic enzyme (Energy pathway)
11	Glutathione S-transferase	XP_857014	27639.3/6.66	15	35.11	Metabolic enzyme (Energy pathway)

	theta 1-like isoform4					
12	Elongation factor 2	XP_533949	77884/6.34	5	47.47	Translation regulatory protein, protein metabolism
13	Septin 11	XP_535616	52111.6/6.24	8	45.17	GTP-binding protein (GTPase activity, cell cycle, vesicle-mediated transport)
14	Fatty acid synthase	XP_540497	268846.4/5.99	2	87.67	Metabolic enzyme (Energy pathway, catalytic activity)
15	Dihydropyrimidinase -related protein 3	XP_544332	94582/7.08	24	275.93	Metabolic enzyme (Energy pathway, hydrolase activity)
16	D-3-phosphoglycerate dehydrogenase-like	XP_849835	56545.8/6.19	17	141.56	Metabolic enzyme (Energy pathway, catalytic activity)
17	Aldehyde dehydrogenase,	XP_853628	56763.1/6.63	25	176.99	Metabolic enzyme (Energy pathway,

	mitochondrial isoform 2 (ALDH2)					catalytic activity)
18	Heterogeneous nuclear ribonucleoprotein K isoform a isoform 1 (HNRNPK)	XP_533511	50890.4/5.31	18	116.18	RNA-binding protein
19	Mitogen-activated protein kinase 1	XP_860750	42880.5/6.28	16	88.01	Signal transduction, cell communication (serine/threonine kinase activity)
20	Not identified					
21	Not identified					
22	Not identified					

† Protein spot numbers corresponded to the two-dimensional gel electrophoresis image in Fig. 1.

‡ Accession code in NCBI.

§ Amino acid coverage (%).

MW, theoretical molecular weight; Da, Daltons; pI, theoretical isoelectric point.

Table 2 Details on patients' age, sex, tumor location, and annexin A2 staining

Case	Age	Sex	Location	Stainability for annexin A2	
				Perivascular tumor cells	Single invasive tumor cells
1	69	M	L. Temporal	++	-
2	67	M	L. Frontal	++	-
3	76	M	L. Frontal	+++	+
4	58	M	L. Frontal	+	-
5	75	M	L. Temporal	+	-